

Scientific paper

# Synthesis and Fluorescent Properties of Chromium-Doped Aluminate Nanopowders

Janez Križan,<sup>1</sup> Janez Možina,<sup>2</sup> Ivan Bajsić<sup>2</sup> and Matjaž Mazaj<sup>3</sup><sup>1</sup> AMI d.o.o., Ptuj, Slovenia<sup>2</sup> Faculty of Mechanical Engineering, University of Ljubljana, Slovenia<sup>3</sup> National Institute of Chemistry, Hajdrihova 19, 1000 Ljubljana, Slovenia

\* Corresponding author: E-mail: matjaz.mazaj@ki.si

Received: 28-08-2011

## Abstract

Nanocrystalline chromium-doped  $\text{Al}_2\text{O}_3$  and  $\text{MgAl}_2\text{O}_4$  products were synthesised by combustion method in the presence of urea. The powders were characterised by X-ray diffraction analysis (XRD), scanning electron microscopy (SEM), BET surface area analysis, induction coupled plasma analysis (ICP) and mapping energy dispersive X-ray analysis (EDX). Fluorescence properties of the products were investigated in order to find the applications in fluorescent sensor and in the production of transparent polycrystalline ceramic materials for laser and optical application.

**Keywords:** Cr-doped alumina, Cr-doped spinel, combustion synthesis, fluorescence

## 1. Introduction

Nanotechnology has become a key area in the development of science and engineering.<sup>1</sup> Nanosized particles (10–100 nm) provide higher surface areas which enable many advantages over the micro-sized materials, special in the fields of catalysis, coating technologies and optics. One of the most frequently used nanosized ceramic material is aluminium oxide with corundum structure type ( $\alpha\text{-Al}_2\text{O}_3$ ). It is widely used in various fields of engineering such as coatings, heat-resistant materials, abrasives and optics due to its hardness, acid/base and water resistance and thermal stability.<sup>2–4</sup> In the field of optical and sensor applications, earth-alkali metal aluminate materials such as spinel ( $\text{MgAl}_2\text{O}_4$ ) and alexandrite ( $\text{BeAl}_2\text{O}_4$ ),  $\text{CaAl}_2\text{O}_4$  and  $\text{SrAl}_2\text{O}_4$  have also been intensively investigated for decades.<sup>5–7</sup> In particular spinel has shown a great potential as a transparent scintillator.<sup>8</sup> Its cubic crystal structure enables good optical transparency in all directions transmitting light from 200 to 5500 nm with no optical distortion.<sup>9</sup> Its mechanical, optical and non-hygroscopic properties are comparable with polycrystalline aluminium oxide. Rare-earth doped alkaline aluminates ( $\text{MAl}_2\text{O}_4\text{:Eu}^{2+}, \text{Dy}^{3+}$ ; M = Mg, Ca, Sr, Ba) exhibit

excellent persistent luminescence properties.<sup>10,11</sup> Among various rare-earth and transition metal used for doping,  $\text{Cr}^{3+}$ -doped aluminates also attracted great interest due to its broad-band luminescence properties at room temperature which makes them applicable as medium for tunable lasers.<sup>12,13</sup>

Here we report on the synthesis of  $\text{Cr}^{3+}$ -doped corundum and spinel nanopowders with high purity and crystallinity by combustion method which has many advantages over the other methods as it is cost-effective, simple and with high production yielding. On the synthesised products fluorescence properties were measured for the purpose of sensor applications.

## 2. Experimental

### 2.1. Synthesis of Chromium Doped $\text{Al}_2\text{O}_3$ Nanopowder

For the synthesis of homogenous alumina nanopowder products with high purity and transparency required for optic and sensor applications, the combustion of aqueous redox mixture of aluminium precursor with the

presence of urea seems to be the proper choice. The synthesis was performed according to the literature.<sup>14</sup> In typical synthesis 9.4 g (25 mmol) of  $\text{Al}(\text{NO}_3)_3 \cdot 9\text{H}_2\text{O}$ , 3.8 g (62.5 mmol) of urea and 0.1 g (0.25 mmol) of  $\text{Cr}(\text{NO}_3)_3 \cdot 9\text{H}_2\text{O}$  was mixed with 15 ml of demineralised water in Pyrex dish and combust with the flame burner at 500 °C with intensive reaction yielding voluminous foamy pink powder. In second step, alumina product was sintered at 1300 °C for 2 hours. For comparison, pure alumina product (without  $\text{Cr}^{3+}$  cations) was prepared identically, with the absence of  $\text{Cr}(\text{NO}_3)_3 \cdot 9\text{H}_2\text{O}$  in the starting reaction mixture.

## 2. 2. Synthesis of Chromium-Doped $\text{MgAl}_2\text{O}_4$ Spinel Nanopowder

Synthesis of Cr-doped spinel nanopowder was performed by combustion of aluminium and magnesium precursors in the presence of urea with the similar method as in the case of alumina synthesis. 18.8 g (50 mmol) of  $\text{Al}(\text{NO}_3)_3 \cdot 9\text{H}_2\text{O}$ , 6.4 g (25 mmol) of  $\text{Mg}(\text{NO}_3)_2 \cdot 6\text{H}_2\text{O}$ , 15.0 g (25 mmol) of urea and 0.1 g (0.25 mmol) of  $\text{Cr}(\text{NO}_3)_3 \cdot 9\text{H}_2\text{O}$  was mixed with 15 ml of demineralised water in Pyrex dish and combust with the flame burner at 500 °C. Note that during the combustion processes the temperature increased rapidly to 1200–1300 °C in both, undoped and Cr-doped syntheses procedures. Voluminous pink powder was sintered at 1300 °C for 2 hours. Only characterisation of the sintered spinel product is described in further text.

## 2. 3. Characterisation

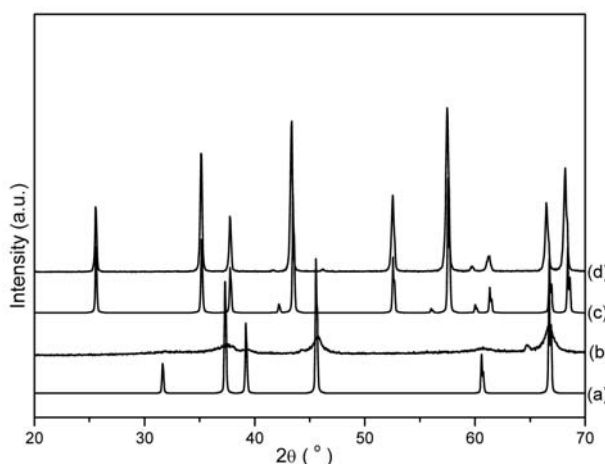
X-ray powder diffraction (XRD) patterns were recorded on a PANalytical X'Pert PRO high-resolution diffractometer with Alpha1 configuration using  $\text{CuK}\alpha$  radiation (1.5406 Å) in the range from 20 to 70° 2 $\theta$  with the step 0.017° per 100 s using fully opened 100 channel X'Celerator detector. Scanning electron microscopy (SEM) was studied on a Zeiss Supra 3VP field-emission microscope operating at 1 kV. Elemental analysis was performed by inductive-coupled plasma atomic emission spectrometry on a Atom Scan 25 (Thermo Jarrell Ash) ICP-AES spectrometer. The distribution of chromium within the products was observed by energy dispersive X-ray analysis mapping (EDX) with an INCA Energy system attached to the above described SEM microscope. Nitrogen adsorption–desorption isotherms were measured at –196 °C using a Tristar 3000 (Micromeritics, Norcross, GA, USA). Before the measurement the samples were outgassed for 12 h at 105 °C and for 2 h at 150 °C in the degas port of the instrument. The BET specific surface area was calculated by using adsorption data in the relative pressure range from 0.05 to 0.16. Emission spectra were excited at 405 nm using LED diodes and measured on an Ocean-Optics USB4000 spectrometer.

## 3. Results and Discussion

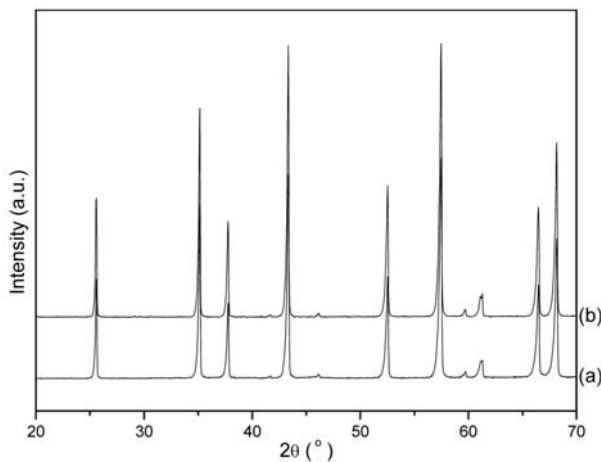
### 3. 1. XRD and SEM Analysis

Figure 1 shows XRD patterns of pure  $\text{Al}_2\text{O}_3$  products before and after sintering procedure. Pyrolysis of aluminium precursor in the presence of urea yields  $\gamma\text{-Al}_2\text{O}_3$  phase. Relatively broad peaks with low intensity indicate the presence of nanosized particles with low degree of crystallinity. SEM micrograph of as-prepared  $\gamma\text{-Al}_2\text{O}_3$  phase shown on Figure 3a indicates the estimated particle size between 20 and 50 nm. Sintering process induces the transformation from  $\gamma\text{-Al}_2\text{O}_3$  to highly crystalline corundum  $\alpha\text{-Al}_2\text{O}_3$  phase. Merging of individual nanoparticles to bulkier particles with the estimated size up to 500 nm (Figure 3b) also contribute to narrower peaks with higher intensities. The values of particle sizes estimated from SEM micrographs are in a good agreement with the ones calculated by Scherrer equation (60 and 370 nm for  $\gamma\text{-Al}_2\text{O}_3$  and  $\alpha\text{-Al}_2\text{O}_3$  phases respectively). In contrast, the pyrolysis of  $\text{Al}^{3+}$ /urea precursor solution in the presence of  $\text{Cr}^{3+}$  cations yields pure and highly crystalline corundum phase already at the first stage (Figure 2) with the size of the particles below 100 nm as can be seen from Figure 3c. Thermal treatment at 1300 °C does not affect the crystal structure of corundum  $\text{Al}_2\text{O}_3$  which remains highly crystalline during the sintering procedure. Merging of Cr-doped alumina nanoparticles with the estimated size up to 50 nm to larger crystallites is observed similarly as in the case of pure alumina products (Figures 3c and 3d). We can conclude that the presence of  $\text{Cr}^{3+}$  cations in precursor solution has a strong influence on formation of  $\text{Al}_2\text{O}_3$  phases and seems to direct the crystallisation of corundum structure during the pyrolysis process.

XRD pattern of chromium-doped  $\text{MgAl}_2\text{O}_4$  product sintered at 1300 °C shown on Figure 4 indicates that the pyrolysis of aluminium and magnesium precursors in the presence of urea and additional thermal treatment leads to



**Figure 1:** Powder XRD patterns of (a) reference  $\gamma\text{-Al}_2\text{O}_3$  (PDF # 010-0425), (b) as-prepared  $\text{Al}_2\text{O}_3$ , (c) reference  $\alpha\text{-Al}_2\text{O}_3$  (PDF # 005-0712) and (d) sintered  $\text{Al}_2\text{O}_3$  products.



**Figure 2:** Powder XRD patterns of Cr-doped (a) as-prepared  $\text{Al}_2\text{O}_3$  and (b) sintered  $\text{Al}_2\text{O}_3$  products.

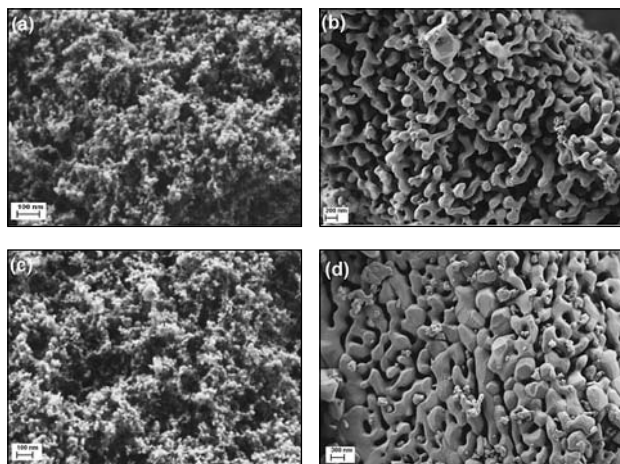


**Figure 3:** SEM micrographs of (a) as-prepared and (b) sintered pure alumina, (c) as-prepared and (d) sintered Cr-doped alumina products.

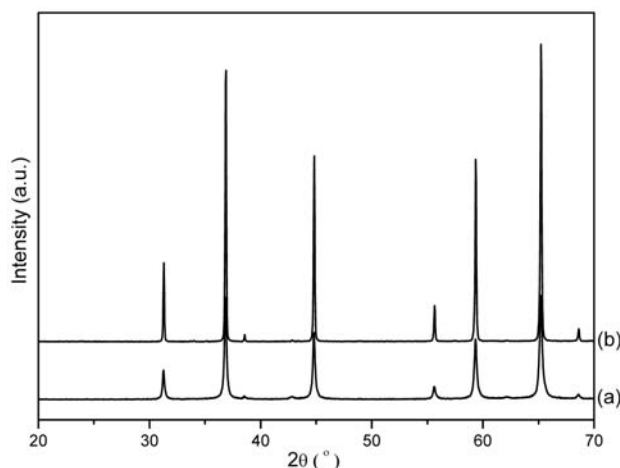


**Figure 4:** XRD pattern of  $\text{Cr}^{3+}$ -doped (a) as-prepared and (b) sintered  $\text{MgAl}_2\text{O}_4$  products.

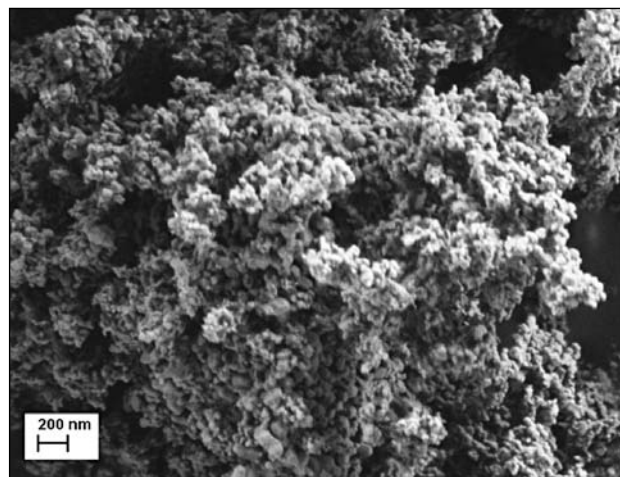


**Figure 5:** SEM micrograph sintered Cr-doped  $\text{MgAl}_2\text{O}_4$  product.

the formation of pure, highly crystalline spinel phase. SEM micrograph shown on Figure 5 indicates the size of the crystals up to 100 nm.

### 3. 2. Elemental and Surface Area Analysis

The amount of chromium doped in corundum and spinel products was investigated by ICP-AES analysis. Doping of  $\text{Cr}^{3+}$  ions seem to be slightly more effective within spinel structure in comparison with corundum. Al/Cr molar ratios were 90 and 58 for sintered Cr-doped alumina and spinel products, respectively. Al/Mg ratios of 1.982 and 1.964 for sintered Cr-doped alumina and spinel confirmed exchange of  $\text{Al}^{3+}$  by  $\text{Cr}^{3+}$  cations and thus effective doping process. To obtain even more information about the distribution of chromium ions within the samples, EDX mapping was performed. To achieve better analysis results, the products were compressed in the self standing pellets and coated with carbon prior analysis in order to avoid excessive charging. Mapping results were collected after 100 minutes of exposure time on a surface area of about  $6 \text{ mm}^2$ . As can be seen from Figure 6, in all products chromium seems to be evenly dispersed throughout the sample, which indicates effective and homogeneous doping within corundum and spinel structures.

Specific surface area was calculated from BET method on the basis of  $\text{N}_2$  isotherms measured at 77 K. As-prepared Cr-doped corundum product has, as expected, the highest surface area since it contains the particles with the smallest dimensions and interparticle porosity becomes important factor for  $\text{N}_2$  adsorption uptake. Surface area drastically decreases after sintering process due to the merging of nanoparticles to bulkier crystals. Surface area of sintered Cr-doped spinel is higher as in the case of sintered  $\text{Al}_2\text{O}_3:\text{Cr}$ , since the sintered spinel particles are somewhat smaller. Chemical composition and surface area properties of  $\text{Al}_2\text{O}_3:\text{Cr}$  and  $\text{MgAl}_2\text{O}_4:\text{Cr}$  are described in the Table 1.

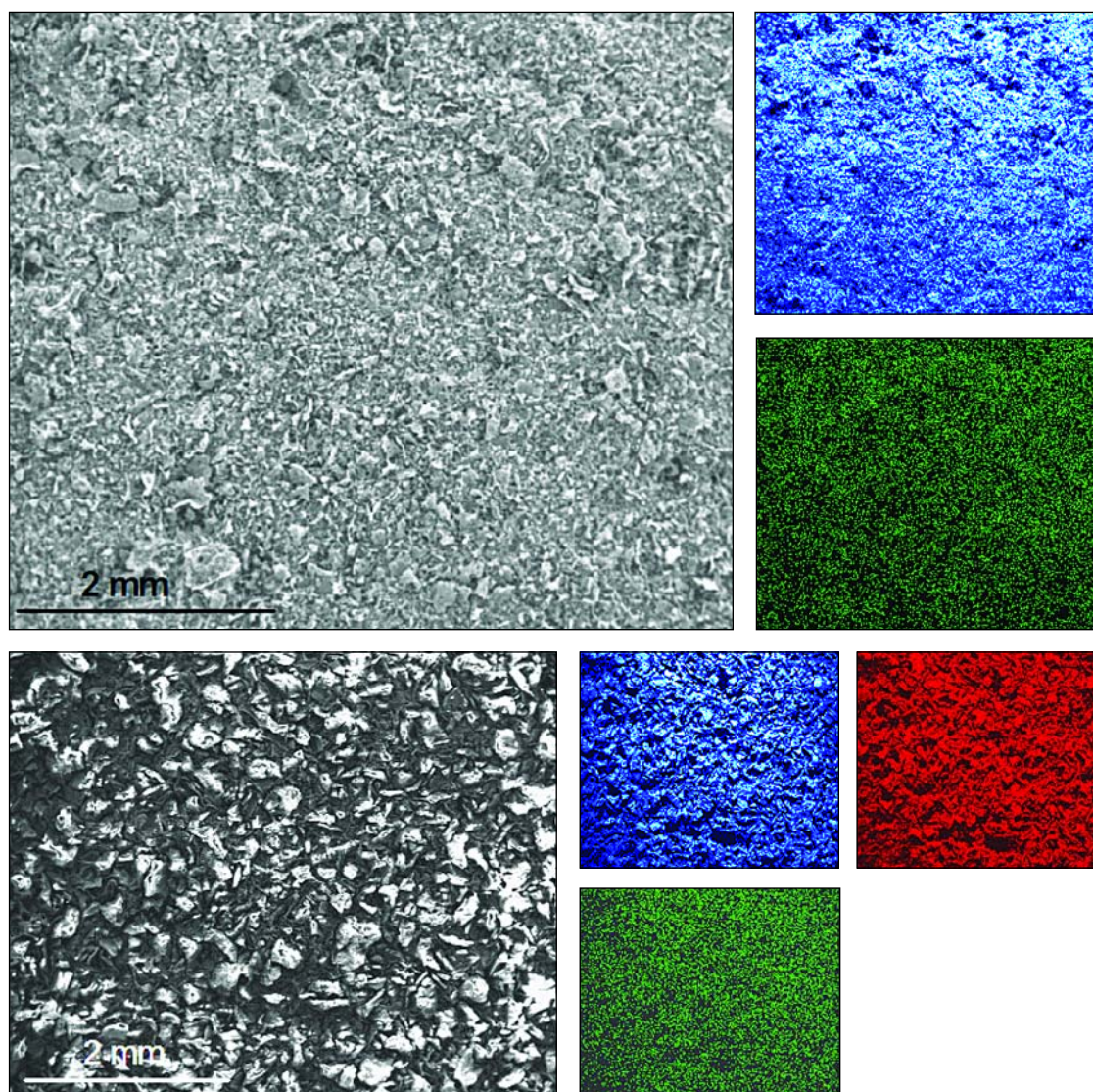


**Figure 6:** EDX mapping analysis of (a) alumina and (b) spinel Cr-doped sintered products. Coloured squares represent the distribution of individual elements throughout the corresponding surface: aluminium (blue), magnesium (red), chromium (green).

**Table 1:** Chemical composition, particle size and surface area properties of as-prepared and sintered  $\text{Al}_2\text{O}_3\cdot\text{Cr}$  and  $\text{Cr}:\text{MgAl}_2\text{O}_4$  products.

product	Chemical composition	particles size (nm)	Specific surface area ( $\text{m}^2/\text{g}$ )
$\text{Al}_2\text{O}_3\cdot\text{Cr}$ (as-prepared)	$(\text{Al}_{1.979}\text{Cr}_{0.021})\text{O}_3$	~ 50	108
$\text{Al}_2\text{O}_3\cdot\text{Cr}$ (sintered)	$(\text{Al}_{1.978}\text{Cr}_{0.022})\text{O}_3$	~ 500	9
$\text{MgAl}_2\text{O}_4\cdot\text{Cr}$ (as-prepared)	$\text{Mg}(\text{Al}_{1.966}\text{Cr}_{0.033})\text{O}_4$	~ 100	20
$\text{MgAl}_2\text{O}_4\cdot\text{Cr}$ (sintered)	$\text{Mg}(\text{Al}_{1.966}\text{Cr}_{0.034})\text{O}_4$	~ 150	29

### 3. 3. Fluorescence Measurements

The fluorescence spectrum of sintered  $\text{Al}_2\text{O}_3\cdot\text{Cr}^{3+}$  corundum at room temperature with the excitation at 405 nm ( $24691\text{ cm}^{-1}$ ) is shown on Figure 7. The most intense band occurs in the red region at 694 nm. There are also two weaker but still distinctive bands at 720 nm and at 670 nm. These bands can be attributed to the  ${}^2\text{E} \rightarrow {}^4\text{A}_2$  transi-

tions of  $\text{Cr}^{3+}$  ions which adopt part of the  $\text{Al}^{3+}$  octahedral positions in corundum crystal structure. The host sensitive 3d orbits of  $\text{Cr}^{3+}$  are split in strong  $\text{Al}_2\text{O}_3$  crystal field and produce the ground level  ${}^4\text{A}_2$  and one of the excited state –  ${}^2\text{E}$ .  ${}^2\text{E}$  represents lowest excited band acting as emitting level. The magnitude of this crystal field splitting extends  ${}^2\text{E}$  state above the ground state. Thus the  ${}^2\text{E} \rightarrow {}^4\text{A}_2$  transi-

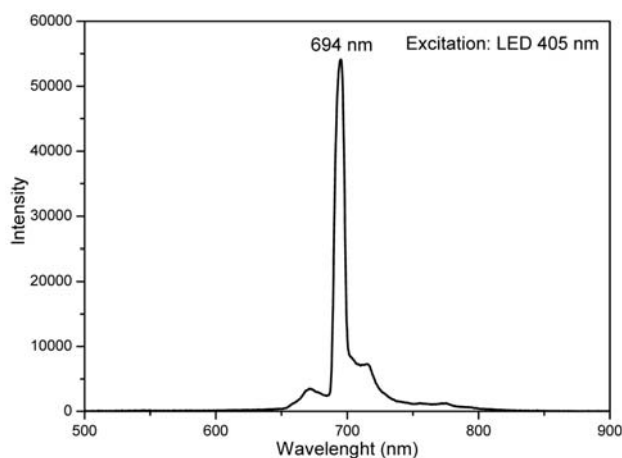


**Figure 7:** Fluorescence spectrum of  $\text{Al}_2\text{O}_3:\text{Cr}^{3+}$  with excitation wavelength at 405 nm.

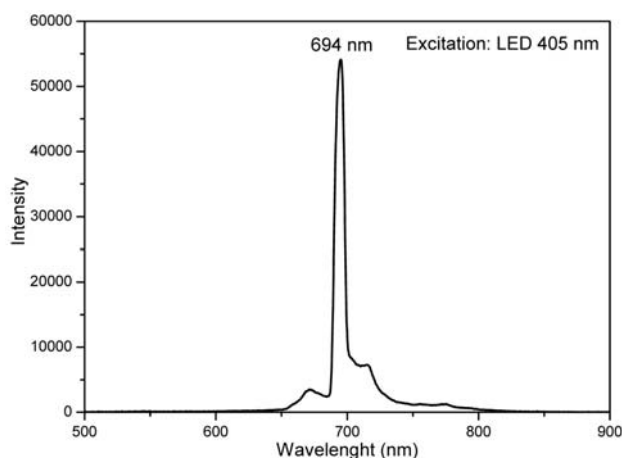


**Figure 8:** Fluorescence spectrum of  $\text{MgAl}_2\text{O}_4:\text{Cr}^{3+}$  with excitation wavelength at 405 nm.

tion of  $\text{Al}_2\text{O}_3:\text{Cr}^{3+}$  crystal lies in visible spectral region with the intense band at 694 nm.<sup>12,15–17</sup> The fluorescence spectrum of sintered  $\text{MgAl}_2\text{O}_4:\text{Cr}^{3+}$  at room temperature, shown on Figure 8 exhibits three characteristic bands with the most intense peak at 689 nm corresponding to  ${}^2\text{E} \rightarrow {}^4\text{A}_2$  spin-forbidden transition of  $\text{Cr}^{3+}$  ions, which occupy some of the  $\text{Al}^{3+}$  octahedral sites in spinel crystal structure. There are also two less intensive and partially overlapped peaks at 677 and 707 nm which could correspond to N-lines (zero-phonon lines) related to a coupling between  $\text{Cr}^{3+}$  state and lattice defects and to  $\text{Cr}^{3+}-\text{Cr}^{3+}$  pair interactions.<sup>17–19</sup>

## 4. Conclusions

Chromium-doped corundum  $\text{Al}_2\text{O}_3$  and spinel  $\text{MgAl}_2\text{O}_4$  nanopowders were synthesised by simple and fast

combustion method of metal precursors in the presence of urea. Phase determination of corundum and spinel was confirmed by XRD, nanosized particles of the prepared products were observed by SEM. Elemental composition determined by EDX indicated even and homogenous distribution of  $\text{Cr}^{3+}$  within corundum and spinel structures with chemical composition corresponding to chemical formulas  $(\text{Al}_{1.978}\text{Cr}_{0.022})\text{O}_3$  and  $\text{Mg}(\text{Al}_{1.966}\text{Cr}_{0.034})\text{O}_4$  respectively. Optical properties of chromium-doped aluminae measured by spectrometer with the excitation line at 405 nm confirmed that cost-effective method leads to the production of fluorescent materials which can be applied in the development of various sensors and new types of polycrystalline ceramic lasers.

## 5. References

1. L. C. Pathak, T. B. Singh, S. Das, A. K. Verma, P. Ramachandrarao, *Mater. Lett.* **2002**, *57*, 380–385.
2. J. Tikkanen, K. A. Gross, C. C. Berndt, V. Pitkanen, J. Keskinen, S. Raghu, M. Rajala, J. Karthikeyan, *Surf. Coat. Technol.* **1997**, *90*, 210–216.
3. K. A. Evans, *Key Eng. Mater.* **1996**, *122–124*, 489–526.
4. M. N. Rittner, *Am. Ceram. Soc. Bull.* **2002**, *81*, 33–36.
5. H. Aizawa, N. Ohishi, S. Ogawa, E. Watanabe, T. Katsumata, S. Komuro, T. Morikawa, E. Toba, *Rev. Sci. Instrum.* **2002**, *73*, 3089–3092.
6. K. T. V. Grattan, A. W. Palmer, Z. Y. Thang, *Rev. Sci. Instrum.* **1992**, *63*, 3869–3872.
7. W. H. Fonger, C.W. Struck, *Phys. Rev. B* **1975**, *11*, 3251–3260.
8. C.-F. Chen, F. P. Doty, R. J. T. Houk, R. O. Loutfy, H. M. Volz, P. Yang, *J. Am. Ceram. Soc.* **2010**, *93*, 2399–2402.
9. D.C. Harris, *Materials for Infrared Windows and Domes: Properties and Performance*, Spie Optical Engineering Press, Bellingham, WA, 1999.
10. K. Van den Eeckhout, P.F. Smet, D. Poelman, *Materials* **2010**, *3*, 2536–2566.
11. V. Abbruscato, *J. Electrochem Soc.* **1971**, *118*, 930–933.
12. W. Mikenda, A. Preisinger, *J. Lumin.* **1981**, *26*, 53–66.
13. T.-L. Phan, S.-C. Yu, *J. Kor. Phys. Soc.* **2004**, *45*, 63–66.
14. J. J. Kingsley, K. C. Patil, *Mater. Letters* **1988**, *6*, 427–432.
15. L.-Y. Yang, Y.-J. Dong, D.-P. Chen, C. Wang, N. Da, X. W. Jiang, C. Zhu, J.-R. Qiu, *Optics Express* **2005**, *13*, 7893–7898.
16. C. Garapon, A. Brenier, R. Moncorgé, *Opt. Mater.* **1998**, *10*, 177–189.
17. A.R. Zanatta, C.T.M. Ribeiro, U. Jahn, S.B. Aldabergenova, H.P. Strunk, *J. Appl. Phys.* **2006**, *100*, 113112.
18. P. J. Derén, M. Malinowski, W. Streck, *J. Lumin.* **1996**, *68*, 91–103.
19. C. Garapon, H. Manaa, R. Moncorgé, *J. Chem. Phys.* **1991**, *95*, 5501–5512.
20. W. Mikenda, A. Preisinger, *J. Lumin.* **1981**, *26*, 67–83.

## Povzetek

Z metodo izgorevanja smo v prisotnosti uree sintetizirali nanokristalinična  $\text{Al}_2\text{O}_3$  (korund) in  $\text{MgAl}_2\text{O}_4$  (spinel) materiala dopirana s kromom. Nedopirani in dopirani produkti korunda in spinela so bili karakterizirani z metodami rentgenske praškovne difrakcije (XRD), vrstične elektronske mikroskopije (SEM), analize specifične površine z BET metodo, analize inducirane sklopljene plazme (ICP) in energijsko disperzivne rentgenske analize (EDX). Na omenjenih materialih smo preiskovali fluorescenčne lastnosti za razvoj prosojnih keramičnih materialov za laserske in senzorske aplikacije.